

We thank the reviewers for their thoughtful and detailed comments. Below we respond to the individual comments.

Reviewer #1

General comments

(1) *This paper reports high resolution inversion of CO emission sources over North America using the nested version of GEOS-Chem model. The authors use the surface level retrievals from the MOPITT version 5 NIR+TIR data product to constrain the inversion. The paper is well written and logically organized in my opinion. The authors provide a useful discussion of the initial and boundary conditions used for the model runs. Further they investigated the sensitivity of the inversion estimates to the OH fields and pointed out the potential issues and how they may be addressed in future work to improve these high resolution inversion analyses. They have also compared results from their inversions with aircraft data from INTEX-A bolstering confidence in their analysis. The research presented in this work is well within the scope of Atmospheric Chemistry and Physics and I recommend publication after revision.*

Thanks for the comments!

Specific Comments:

(1) *While an impressive amount of work has gone into this paper, it will be nice to have a better understanding of some of their main results. In Figure 5, the authors show extensive areas in North America with strongly decreased a posteriori emissions in summer and attribute this to the oxidation of the biogenic VOCs there being a high bias of isoprene emissions in MEGAN 2.0 inventory that they have used for their simulations. If the summer decrease is due to high bias in isoprene emissions, then the spatial distribution of this anomaly should correspond to the observed isoprene spatial distribution. The isoprene distribution as deduced from HCHO retrievals from OMI shows a strong plume in summer essentially over the South Eastern US (Millet et al. 2008), and much less over the extensive areas in the western US going down to Mexico where the authors show strongly decreased a posteriori emissions (in addition to SE US) as can be seen in Figure 5, particularly between July and September. Therefore it is not clear to me if the wide spread discrepancy in CO emissions in summer can all be explained simply in terms of isoprene high bias in MEGAN 2.0. In any case, I believe the latter is now obsolete and the MEGAN version 2.1 with updates is available. Indeed in a recent paper, Hu et al., (2015, JGR, in press) used a similar high resolution nested grid version of GEOS-Chem with MEGAN 2.1 and found that the model adequately simulates*

the isoprene observations near a site in US upper Midwest. I would therefore urge the authors to redo their analysis using this updated inventory.

The MEGANv2.1 inventory does reduce the overestimate in the isoprene emissions found in MEGANv2.0. However, as we noted in Jiang et al. (2015), with MEGANv2.1 GEOS-Chem still overestimates emissions in South America and Africa. It seems as though a key improvement in the implementation of the MEGANv2.1 inventory in Hu et al. (2015) is the use of a new land cover scheme. The resulting simulation does lead to a significant improvement in the modeled isoprene over North America. We now cite the Hu et al. (2015) paper in the manuscript. Unfortunately, this implementation of the MEGANv2.1 inventory is not yet available in the GEOS-Chem adjoint model so we cannot redo the analysis with the updated inventory.

We also believe that reduction in the emissions in Mexico and the southern US will, in part, be driven by the bias in the southern boundary conditions, which is associated with outflow from South America. We have added text in Sections 4.1 (at the end) and 4.2 (in the first paragraph) explaining this.

(2) I find it very interesting that several city scale features are showing up nicely in this plot. The authors mentioned about Toronto. More prominent are two persistent features over the Mexico City area and perhaps Monterrey for most of the year with low a posteriori emissions, except spring. The authors should discuss this—with the large amount of data over the Mexico City area from all the field missions and ground based measurements, it should be possible to find an explanation for the low a posteriori.

The top-down constraints on small-scale features are indeed interesting but it is important that we not overly interpret the results. As we noted in the paper, it is unclear how reliable these features are, given the information content of the MOPITT data. For example, using the nested GEOS-Chem model to carry out an inversion analysis of GOSAT CH₄ data, Turner et al. (ACPD, doi:10.5194/acpd-15-4495-2015) estimated that the inversion produced only 39 independent pieces of information on the methane distribution (degrees of freedom for signal (DOFs)) across North America. Although, given the greater variability in the distribution of CO, we would expect more DOFs in the MOPITT inversion. If the DOFs is small, it means that the information came from the prior rather than the observations. Ideally, using the prior and posterior error covariance matrices we can estimate the contributions from the prior and from the observations. However, we believe that until we conduct such an analysis to quantify the DOFs in the inversion, it would be premature to emphasize the city-scale source estimates.

(3) I am also a little intrigued that Kopacz et al. (2010) did not find any required adjustment over the entire US and Central America area in summer. Since the authors

compare their results with Kopacz et al. (2010) for the same time period, they should add a discussion explaining this difference for the sake of completeness.

We did a detailed comparison between our analysis with Kopacz et al. (2010) in our global-scale inversion paper (Jiang et al. 2015). As we noted in Jiang et al. (2015), Kopacz et al. (2010) used much lower priori emissions, reflecting the significant (60%) summertime reduction in CO emissions recommended by Hudman et al. (2008) (see the discussion at the end of Section 4.1 in Jiang et al., 2015). Also, as noted in Jiang et al. (2015), the contributions from local VOC emissions were not included in the state vector in the Kopacz et al. (2010) inversion analysis. They aggregated the isoprene source with the methane source and optimized solved for global mean source from methane and VOC oxidation. Rather than duplicating what is already in the literature, we have added the following text to the manuscript: “As discussed in Jiang et al. (2015), the seasonal variations of the a posteriori source estimates obtained here are consistent with those of Kopacz et al. (2010), but the magnitude of the sources estimates differ significantly, reflecting differences in the configuration of the inversions analyses. We refer the reader to Jiang et al. (2015) for a more detailed discussion of the differences between the source estimates obtained here and those from Kopacz et al. (2010).”

Technical Comments:

(1) *There are several discrepancies in the references:*

a) The reference Kilch et al., 2014 is not listed in the references. The authors likely mean the paper by Klich and Fuelberg which is listed. b) Palmer et al. 2003 missing in the reference list c) Kopacz et al., 2009 missing in the reference list d) Liu and Nocedal, 1989 year (2010) is wrong in the reference list.

Changed.

2. Figure 5 readability will be better if the x axis labels (latitude) are given only for the bottom panels. Further, the color scale may be changed so as to discriminate $f=1$ more clearly (say white, as in Kopacz et al. ,2010).

Changed.

3. Figure 1 will look better with color scales placed vertically.

Changed.

4. Figure 4 color bar for column CO should be placed on top of the figures alternately, put all the 3 CO column maps (Figure 4a-c) in one row and Fig 4d in a different row.

We have split the figure into Figures 4 and 5.

5. *I think the authors need to use a consistent terminology for the sign of the source estimate. for instance, I found the sentences (page 5338) “ The estimated winter emissions of Kopacz et al.(2010) are about 20% larger than the summer emissions. Kopacz et al (2010) and Stein et al. (2014) attributed the low bias of northern hemisphere CO in winter to an underestimation of road traffic emission” to be somewhat confusing.*

Thanks! The text has been adjusted.

Reviewer #2

General comments

(1) *This paper presents a regional (N. America) inversion of CO fluxes using MOPITT observations and the GEOS-Chem CTM. The main thesis of the paper is that a high resolution regional inversion, with proper boundary conditions, can overcome some of the major difficulties facing CO flux inversion. These are transport and prescribed OH errors, which can contaminate the inversion results if they are very large.*

This is a well written and easy to follow paper, and I recommend a minor revision before the paper is published. My main comments (described in more detail below), are that some further analysis of the errors would be helpful, particularly in the comparisons with in situ data.

Thanks for the comments!

Specific comments

(1) *P. 5336, line 5. It would be useful to know how these differences vary with height, and how they compare with in situ measurements. Do higher altitude differences have larger differences (because of the impact of long range transport)?*

P. 5336, lines 24-26. Similarly, it would be good to know more about how these differences vary with altitude. Can comparisons with in situ observations bet shown here (in the same format as panel (d))? This can help to understand how the boundary conditions are affected by long range transport.

Thanks for your suggestion! The bias is largest in the southern boundary and we now include a figure (Figure 6) showing the vertical distribution of the relative differences

between the model and MOPITT. There are large positive biases in lower troposphere and negative biases in upper troposphere, in the vicinity of the outflow of biomass burning emissions from South America. Liu et al. (2010) conducted an evaluation of the GEOS-Chem model in this region using data from TES and MLS. We have added a paragraph at the end of Section 4.1 discussing this and summarizing the results of Liu et al. (2010).

Regarding the use of in situ data, in Figure 9 we compare the model with aircraft data from the INTEX-A campaign. The Kalman filter produces initial and boundary conditions (our a priori) with a small bias of 7.2 ppb relative to the in situ data in the free troposphere (Figure 9a)

(2) Also (from P. 5336) the use of MOPITT CO retrievals for the initialization and boundary conditions should make the a priori correlated with MOPITT observation errors. How will this affect the inversion results, given that it is generally assumed that model and observations are uncorrelated?

The inversion is linear and across North America the CO state (distribution) reflects a background contribution, transported from lateral boundaries and the initial state, and a location contribution from fresh North American emissions. (Fresh here means since the beginning of the assimilation period.) Use of the MOPITT data to optimize the initial and boundary conditions means that the background contribution of the state will be correlated with the MOPITT data. That is not a problem since our objective is to “remove” that background influence in the context of the inversion, so that model-data mismatch in the cost function, Eq. (2), will be dominated by the perturbations to the state associated with fresh North America emissions. In this approach, we use the MOPITT data to adjust the fresh North American emissions and not the influence of the initial and boundary conditions.

(3) P. 5339, lines 11-21. It would also help the error analysis to show how the differences with INTEX-B (and perhaps adding NOAA aircraft data) vary with altitude. It seems that if the inversion is relatively unbiased, then the errors should be smaller near the surface, and become larger at higher altitudes where transport errors become important.

Actually, we expect the bias to be larger in the boundary layer because we are using optimized boundary and initial conditions, in which we are forcing the model to match the MOPITT data on the boundaries and at the beginning of the inversion period. As mentioned above, in this approach, the largest model-data mismatch in the cost function will be near the fresh source emissions in the domain. Unfortunately, as shown in Figure 6 in the revised manuscript, there is a large transport bias in the southern boundary. However, despite this discrepancy on the southern boundary, the mean bias relative to the aircraft data across North America is small, 7.2 ppb. The inversion further reduces this,

suggesting that transport within North America is unbiased in the model. If the vertical transport over North America were biased the inversion would degrade the agreement with independent data that was obtained with the optimized initial and boundary conditions. We have added text at the end of Section 4.2 explaining this.

1 **Regional data assimilation of multi-spectral MOPITT observations of CO**
2 **over North America**

3
4 Zhe Jiang^{1,2}, Dylan B. A. Jones^{1,3}, John Worden², Helen M. Worden⁴, Daven K. Henze⁵, Yuxuan
5 Wang^{6,7}

6 ¹Department of Physics, University of Toronto, Toronto, ON, Canada, ²Jet Propulsion
7 Laboratory, California Institute of Technology, Pasadena CA, USA, ³JIFRESSE, University of
8 California, Los Angeles, Los Angeles, CA, USA, ⁴National Center for Atmospheric Research,
9 Boulder, CO, USA, ⁵University of Colorado Boulder, CO, USA, ⁶Department of Marine
10 Sciences, Texas A&M University at Galveston, Galveston, TX, USA, ⁷Ministry of Education
11 Key Laboratory for Earth System Modeling, Center for Earth System Science, Institute for
12 Global Change Studies, Tsinghua University, Beijing, China

13
14
15 **Abstract**

16 Chemical transport models (CTMs) driven with high-resolution meteorological fields can
17 better resolve small-scale processes, such as frontal lifting or deep convection, and thus improve
18 the simulation and emission estimates of tropospheric trace gases. In this work, we explore the
19 use of the GEOS-Chem four-dimensional variational (4D-Var) data assimilation system with the
20 nested high-resolution version of the model (0.5°x0.67°) to quantify North American CO
21 emissions during the period of June 2004 – May 2005. With optimized lateral boundary
22 conditions, regional inversion analyses can reduce the sensitivity of the CO source estimates to
23 errors in long-range transport and in the distributions of the hydroxyl radical (OH), the main sink
24 for CO. To further limit the potential impact of discrepancies in chemical aging of air in the free
25 troposphere, associated with errors in OH, we use surface level multispectral MOPITT CO
26 retrievals, which have greater sensitivity to CO near the surface and reduced sensitivity in the
27 free troposphere, compared to previous versions of the retrievals. We estimate that the annual

28 total anthropogenic CO emission from the contiguous US 48 states was 97 Tg CO, a 14%
29 increase from the 85 Tg CO in the a priori. This increase is mainly due to enhanced emissions
30 around the Great Lakes region and along the west coast, relative to the a priori. Sensitivity
31 analyses using different OH fields and lateral boundary conditions suggest a possible error,
32 associated with local North America OH distribution, in these emission estimates of 20% during
33 summer 2004, when the CO lifetime is short. This 20% OH-related error is 50% smaller than the
34 OH-related error previously estimated for North American CO emissions using a global
35 inversion analysis. We believe that reducing this OH-related error further will require integrating
36 additional observations to provide a strong constraint on the CO distribution across the domain.
37 Despite these limitations, our results show the potential advantages of combining high-resolution
38 regional inversion analyses with global analyses to better quantify regional CO source estimates.

39

40 **1. Introduction**

41 Inverse modeling is a powerful tool to improve our understanding of emissions of
42 greenhouse gases and pollutant tracers, by combining observations of atmospheric composition
43 with models. Despite more than a decade of inverse modeling work to better quantify emissions
44 of atmospheric CO (e.g., Palmer et al., 2003; Pétron et al., 2004; Heald et al., 2004; Arellano et
45 al., 2006; Jones et al., 2009; Kopacz et al., 2010; Gonzi et al., 2011; Fortems-Cheiney et al.,
46 2012), there is significant uncertainty in regional CO source estimates, reflecting varying source
47 estimates from the inverse modeling analyses. As noted in previous studies, the discrepancies
48 between the estimated CO emissions from different inversion analyses are due, in part, to errors
49 in the atmospheric models used in the inversions. Model errors in long-range transport, vertical
50 convective transport, diffusion, and chemistry (e.g. Arellano et al. 2006; Fortems-Cheiney et al.,

51 | 2011; [Locatelli et al., 2013](#); [Worden et al., 2013](#); [Jiang et al., 2011, 2013, 2015](#)) all adversely
52 | impact the inverse modeling of CO and other trace constituents (such as methane), and
53 | mitigating these errors in global models is challenging.

Zhe Jiang 6/6/2015 10:30 AM
Deleted: Jiang et al., 2013;
Zhe Jiang 6/6/2015 10:30 AM
Deleted: 2014

54 | One way to reduce the effects of some model errors is to carry out the model simulations
55 | at high spatial resolution, which allows an improved description of small-scale processes,
56 | particularly those associated with vertical convection and diffusion. There have been several
57 | studies using high-resolution mesoscale models for inversion analyses (e.g. [Stroud et al. 2011](#);
58 | [Valin et al. 2011](#); [Klich and Fuelberg 2014](#); [Stock et al. 2014](#)) with the lateral boundary
59 | conditions provided from global, coarse resolution models (e. g. [Curci et al., 2010](#); [Peylin et al.,](#)
60 | [2011](#)). However, the consistency of boundary conditions becomes a critical issue in these
61 | regional analyses (e.g. [Gockede et al., 2010](#)). The boundary conditions have also been imposed
62 | based on independent data, such as aircraft in-situ measurements (e.g. [Brioude et al., 2012](#);
63 | [Lauvaux et al. 2012](#); [Wecht et al. 2014](#)).

Zhe Jiang 6/6/2015 10:30 AM
Deleted: Klich et al.

64 | Regional inverse modeling of CO emissions with adequate boundary condition
65 | optimization will also reduce the impact of discrepancies in long-range transport and in the
66 | chemical sink of CO. Reducing the sensitivity to the chemical sink of CO also requires that
67 | transport across the regional domain is fast compared to the lifetime of CO. [Jiang et al. \(2015\)](#)
68 | compared CO source estimates inferred from inversion analyses of surface level and profile
69 | retrievals of CO from the MOPITT (Measurement of Pollution in The Troposphere) satellite
70 | instrument and found that they were generally consistent (to within 10%), except for source
71 | estimates for North America, Europe, and East Asia. In an earlier study, [Jiang et al. \(2013\)](#) noted
72 | that when comparing source estimates inferred from in situ surface data and from satellite
73 | observations, “in the absence of transport bias, the surface and satellite data should provide

Zhe Jiang 6/6/2015 10:30 AM
Deleted: 2014

78 consistent constraints on the sources, if the data coverage is representative of the spatiotemporal
79 variability in CO". They were the first to show a large discrepancy in the Asian source estimates
80 obtained from the MOPITT surface level and profile retrievals, and they argued that it was due to
81 errors in convective transport over Asia associated with the Asian summer monsoon. In addition
82 to transport biases, discrepancies in the chemical sink of CO will also impact the constraints on
83 the surface sources provided by the surface level and free tropospheric data. Jiang et al. (2015)
84 suggested that the differences in the North American and European sources that they estimated
85 from the MOPITT surface level and profile retrievals could be due to the fact that air in the free
86 troposphere over North America and Europe is more chemically aged, thus, the surface level and
87 profile data are sampling air with different CO characteristics, with the profile data being more
88 susceptible to biases in the chemical sink.

Zhe Jiang 6/6/2015 10:30 AM
Deleted: 2014

89 The work presented here is based on the global analysis of Jiang et al. (2015), but
90 employs the high-resolution, regional version of GEOS-Chem (e.g. Wang et al., 2004; Chen et
91 al., 2009) and the MOPITT surface level retrievals to better quantify North American emissions
92 of CO. We focus on the period June 2004 to May 2005 for consistency with Jiang et al. (2015)
93 and Kopacz et al. (2010). As mentioned above, regional inversion analyses are sensitive to the
94 lateral boundary conditions, but use of global models to provide these boundary conditions is
95 problematic if there are biases in transport and the chemistry in the models. Use of in situ
96 observations to provide boundary conditions is also problematic because observational coverage
97 is often limited in space and time. A better approach for imposing the boundary conditions is to
98 assimilate satellite observations that can provide a strong constraint on the distribution of CO
99 throughout the free troposphere. Here we explore the use of the MOPITT data to constrain the
100 lateral boundary conditions as well as the surface CO emissions. We also examine the potential

Zhe Jiang 6/6/2015 10:30 AM
Deleted: 2014

Zhe Jiang 6/6/2015 10:30 AM
Deleted: 2014

104 impact of discrepancies in the abundance of the hydroxyl radical (OH), the main CO sink, on the
105 estimates CO sources in a regional inverse modeling context.

106 This paper is organized as follows: in Section 2 we describe the MOPITT instruments
107 and the GEOS-Chem model. In Section 3 we outline the inversion framework used in this work.
108 In Section 4, we describe our approach for initial and boundary condition optimization, and
109 present the estimated monthly mean North American emissions. The sensitivity of the source
110 estimates to the chemical sink is examined by comparing the inversion results obtained with two
111 different OH fields. Our conclusions are then provided in Section 5.

112 **2. Observations and Model**

113 **2.1. MOPITT**

114 The MOPITT instrument was launched on December 18, 1999, on NASA's Terra
115 spacecraft. We employ the multispectral version 5 (V5J) retrievals, in which the thermal infrared
116 (TIR) radiances at 4.7 μ m are combined the near infrared (NIR) radiances at 2.3 μ m to provide
117 greater sensitivity to lower tropospheric CO over land (Worden et al., 2010; Deeter et al., 2011).
118 The retrievals are conducted with respect to the logarithm of the volume mixing ratio (VMR),
119 and are reported on a 10-level pressure grid (surface, 900, 800, 700, 600, 500, 400, 300, 200, and
120 100 hPa). Although we use only the surface level MOPITT retrievals in our analysis, it is
121 necessary to transform the modeled CO profile to account for the vertical resolution of the
122 MOPITT retrieval. This transformation is carried out using the following observation operator

$$123 \quad F(\mathbf{x}) = \mathbf{y}_a + \mathbf{A}(H(\mathbf{x}) - \mathbf{y}_a) \quad (1)$$

124 where \mathbf{A} is the MOPITT averaging kernel, $H(\mathbf{x})$ is the GEOS-Chem profile of CO (interpolated
125 onto the MOPITT retrieval grid), and \mathbf{y}_a is the MOPITT a priori profile. After transforming the

126 modeled profile, the modeled CO at the surface is compared to the surface level MOPITT CO, as
127 described in Eq (2) in Section 3. Deeter et al. (2012, 2013) evaluated the multispectral MOPITT
128 data and reported a small positive bias of 2.7% at the surface and a larger positive bias of 14% at
129 200 hPa for the V5J data. The large bias in the upper troposphere is not an issue here since we
130 focus on the surface level data. Further details for the MOPITT instrument and the multispectral
131 retrievals are given in Jiang et al. (2015).

Zhe Jiang 6/6/2015 10:30 AM

Deleted: 2014

132 2.2. GEOS-Chem

133 The GEOS-Chem global chemical transport model (CTM) (<http://www.geos-chem.org>) is
134 driven by assimilated meteorological fields from the NASA Goddard Earth Observing System
135 (GEOS-5) at the Global Modeling and data Assimilation Office. The standard GEOS-Chem
136 chemical mechanism includes 43 tracers, and simulates a detailed description of tropospheric O₃-
137 NO_x-hydrocarbon chemistry, including the radiative and heterogeneous effects of aerosols. The
138 native horizontal resolution of GEOS-5 is 0.5°x0.667°, but the meteorological fields are usually
139 degraded to 4°x5° or 2°x2.5° for global-scale simulations.

140 Our analysis is based on the CO-only simulation in GEOS-Chem v8-02-01, with relevant
141 updates through v9-01-01, using archived monthly OH fields from the full chemistry run. The
142 standard OH field used in this work is from GEOS-Chem version v5-07-08 (Evans et al. 2005).
143 In order to study the influence of the OH distribution on the inversion analyses, we also archive
144 the OH fields from a v8-02-01 GEOS-Chem full chemistry simulation. Additional details about
145 OH fields and emission inventories can be found in Jiang et al. (2015). Briefly, the annual North
146 America sources of CO are 134 Tg CO from fossil fuel and biofuel combustion and biomass
147 burning, 61 Tg CO from the oxidation of biogenic volatile organic compounds (VOCs), and 71
148 Tg CO from the oxidation of CH₄. [Figure 1](#) shows the distribution of the annual mean CO

Zhe Jiang 6/6/2015 10:30 AM

Deleted: 2014

Zhe Jiang 6/6/2015 10:30 AM

Deleted: Fig

152 emissions for June 2004 to May 2005.

153 The inversion analyses here are carried out using the GEOS-Chem four-dimensional
154 variational (4D-Var) data assimilation system, which was first described by Henze et al. (2007)
155 and has been widely used in the chemical assimilation of CO and other tracer gases (e.g. Kopacz
156 et al., 2009, 2010; Singh et al., 2011, Wells et al., 2014, Deng et al. 2014). Previous GEOS-
157 Chem CO inversion analyses were conducted with the global version of the model. Here we
158 extend the 4D-Var system to enable regional inverse modeling of CO using the nested version of
159 GEOS-Chem.

160 The nested capability was first implemented in GEOS-Chem by Wang et al. (2004) for
161 the GEOS-3 version of the meteorological fields. The model was then updated by Chen et al.
162 (2009) to support the GEOS-5 meteorological fields, with $0.5^\circ \times 0.667^\circ$ resolution, which are used
163 here. In the nested simulation the boundary conditions are based on fields archived from a global
164 simulation (at $4^\circ \times 5^\circ$ or $2^\circ \times 2.5^\circ$) with a 3-hour temporal resolution, which are used to rewrite the
165 tracer concentrations in a buffer zone around the nested domain before every transport step.
166 Along the boundary of the nested domain, the direction of the wind field is used to identify
167 whether the flow is directed into or out of the domain, and the mixing ratios of the tracers in the
168 buffer zone are used to provide the necessary upstream information. A key benefit of using the
169 nested model was shown by Wang et al. (2004), who found that the CO mixing ratios in the
170 high-resolution nested simulation were lower than in the coarse resolution global model, which
171 they attributed to the failure of the coarse global model to capture subgrid vertical motions.

172 [Figure 2](#) shows the simulated CO mixing ratio on May 1, 2006, obtained with the $4^\circ \times 5^\circ$ global
173 simulation and with the nested North America simulation. The yellow box in [Figure 2](#) indicates
174 the buffer zone in which the boundary conditions are applied. As shown in the figure, the high-

Zhe Jiang 6/6/2015 10:30 AM

Deleted: Fig

Zhe Jiang 6/6/2015 10:30 AM

Deleted: Fig

177 resolution CO distribution better reflects the influence of the mid-latitude cyclone present over
178 central North America, and the urban emission centers can be more clearly identified in the high-
179 resolution simulation.

180 3. Inversion Approach

181 The inverse method seeks an optimal estimate of the CO sources that is consistent with
182 both the observed atmospheric concentrations and the a priori constraints on the sources by
183 minimizing the cost function $J(\mathbf{x})$,

$$184 \quad J(\mathbf{x}) = \sum_{i=1}^N (F_i(\mathbf{x}) - \mathbf{y}_i)^T \mathbf{S}_{\Sigma}^{-1} (F_i(\mathbf{x}) - \mathbf{y}_i) + (\mathbf{x} - \mathbf{x}_a)^T \mathbf{S}_a^{-1} (\mathbf{x} - \mathbf{x}_a) \quad (2)$$

185 where \mathbf{x} is the state vector of emissions, N is the total number of observations assimilated over
186 the assimilation window (which is one month), \mathbf{y}_i is the i th vector of observed concentrations
187 (the MOPITT surface level retrievals), and $F(\mathbf{x})$ is the forward model, which accounts for the
188 vertical smoothing of the MOPITT retrieval and is described in Eq. 1. Here \mathbf{x}_a is the a priori
189 estimate and \mathbf{S}_{Σ} and \mathbf{S}_a are the observational and a priori error covariance matrices, respectively.

190 The first term on the right in Eq 2 represents the mismatch between the simulated and observed
191 concentrations weighted by the observation error covariance. The second term represents the
192 departure of the estimate from the a priori. The cost function is iteratively minimized using the
193 L-BFGS algorithm (Liu and Nocedal, 1989). The inversion approach is exactly the same as

194 | described in Jiang et al. (2015). We, therefore, refer the reader to Jiang et al. (2015) for details of
195 the optimizing scheme, the MOPITT data selection criteria, and the specification of the error
196 covariance matrices. We employed an Observing System Simulation Experiments (OSSE) to
197 evaluate our high-resolution 4D-Var system in the Appendix, which suggested the nested
198 inversion has similar reliability as the global scale assimilation system.

Zhe Jiang 6/6/2015 10:30 AM

Deleted: 2014

Zhe Jiang 6/6/2015 10:30 AM

Deleted: 2014

201 **4. Results and Discussion**

202 **4.1. Optimization on the initial and boundary conditions**

203 | We produce initial conditions following the approach of Jiang et al. (2015), by
204 | assimilating MOPITT V5J tropospheric profile data using the sequential sub-optimal Kalman
205 | filter (Parrington et al. 2008) from 1 January 2004 to 1 May 2005. Because of the bias in the V5J
206 | data at 200 hPa, we assimilate the profile data only below 200 hPa. The optimized CO
207 | distribution from the Kalman filter is archived at the beginning of each month, providing the
208 | initial conditions at the beginning of each month for the 4D-Var inversion analyses.

209 | As mentioned above, the lateral boundary conditions for the nested simulation could be
210 | specified from the global model. However, a better approach would be to constrain the global-
211 | scale and regional-scale emissions within the same inversion framework, so that the optimized
212 | emissions on the global-scale will provide less biased boundary conditions for the regional
213 | inversion. Such an approach has been used to constrain CH₄ and N₂O emissions over South
214 | America and Europe (Meirink et al., 2008; Bergamaschi et al., 2010; Corazza et al., 2011) with
215 | the nested TM5 model. An issue with this approach is that the adjustment in the emissions on the
216 | global scale will have to be projected through long-range transport to the nested domain. If there
217 | are any biases in the model transport, those biases will also be projected onto the nested
218 | inversion.

219 | Because the GEOS-Chem nesting is one-way, we cannot implement the same approach
220 | that is used in TM5. Instead, we conduct a global-scale inversion analysis and use the a posteriori
221 | CO fields as boundary conditions for the regional inversion. The a posteriori simulation from the
222 | global scale inversion should provide less biased boundary conditions for the regional scale
223 | inversion than the free running model (without assimilation). However, as mentioned above, the

Zhe Jiang 6/6/2015 10:30 AM

Deleted: 2014

225 boundary conditions could potentially be problematic if there are biases in the model transport.
226 Alternatively, one could optimize the model CO distribution (using the sequential sub-optimal
227 Kalman filter, for example), over writing any potential discrepancy in the tracer distribution
228 associated with errors in the model transport (or chemistry). Here we compare the CO
229 distribution obtained from optimizing the CO distribution using the Kalman filter and from
230 optimizing the CO sources using the 4D-Var system.

231 The relative differences in the CO distribution obtained from these two assimilation
232 approaches are shown in [Figure 3](#). The assimilation of the MOPITT tropospheric profiles with
233 the sequential sub-optimal Kalman filter from January 1 2004 to June 1 2005 is referred as
234 CO_KF. The a posteriori CO distribution obtained from optimizing the monthly mean CO
235 emissions using the 4D-Var scheme is referred as CO_EMS. Shown in [Figure 3](#) are the relative
236 differences of the lower tropospheric (surface – 500 hPa) partial columns, calculated as
237 $(CO_EMS - CO_KF) / CO_KF$. Since both approaches used the same initial conditions,
238 archived from the Kalman Filter assimilation, at the beginning of each month, the relative
239 differences shown in [Figure 3](#) can be considered as the residual bias in the a posteriori simulation
240 that cannot be effectively removed within the one-month assimilation period by adjusting only
241 the surface emissions. The most significant feature is the positive residual bias along the
242 Intertropical Convergence Zone (ITCZ), suggesting errors in convective transport in the model
243 (e.g., Jiang et al., 2013; Worden et al., 2013).

244 Since the objective of this work is to constrain the North American CO emissions, using
245 CO_EMS for the boundary conditions may lead to biases in Mexico, the southern US, and along
246 the North American west coast. Consequently, we decided to use the a posteriori fields from the
247 Kalman filter as our optimized boundary conditions. The impact of the initial and boundary

Zhe Jiang 6/6/2015 10:30 AM

Deleted: Fig

Zhe Jiang 6/6/2015 10:30 AM

Deleted: Fig

Zhe Jiang 6/6/2015 10:30 AM

Deleted: Fig

Zhe Jiang 6/6/2015 10:30 AM

Deleted: There are also large regional differences (positive and negative) in both hemispheres that vary from month to month that are likely due to errors in chemistry and transport. For example, there are significant differences over Central America and the Gulf of Mexico in June – September 2004.

258 | conditions from the Kalman filter assimilation is shown in [Figure 4](#). Driven with original initial
259 | and boundary conditions (without assimilation), the modeled CO columns (Figure 4b) are
260 | obviously lower than that of the MOPITT observations [over the North America continent](#). The
261 | difference [over the continent](#) is much smaller when the initial and boundary conditions are
262 | optimized ([Figure 4c](#)) with the assimilation of the MOPITT profiles. It is clear that a significant
263 | bias will be introduced in the a posteriori regional emission estimates if the original initial and
264 | boundary conditions were used in the inversion analyses. [As](#) described in Jiang et al. ([2015](#)), we
265 | do not assimilate MOPITT data at high latitudes due to a potential positive bias in the CO
266 | retrievals at high latitudes; we only assimilate MOPITT data equator-ward of 40° over oceans
267 | and 52° over land, as shown in [Figure 4](#).

268 | The distribution of the relative differences between the modeled and observed CO fields
269 | is shown in [Figure 5](#). With both the free running model and the optimized initial and boundary
270 | conditions, the distribution of the differences with respect to the MOPITT data are approximately
271 | Gaussian. The free running model has a low bias of -13.3%. Assimilating the MOPITT profile
272 | data to optimize the initial and boundary conditions reduced the mean bias to 3.5%, which
273 | should produce a better constraint on local North American emissions.

274 | [Although the mean a posteriori bias in the initial and boundary conditions is small, the](#)
275 | [largest residual bias in the boundary conditions is found on the southern boundary \(near 10°N\),](#)
276 | [where the a posteriori bias can be as large as 20% \(between 80°W – 100°W\). The vertical](#)
277 | [distribution of the relative bias along the southern boundary is shown in Figure 6. In lower](#)
278 | [troposphere, the original model simulation has a large positive bias \(Figure 6a\), approaching](#)
279 | [50%, which the Kalman Filter assimilation significantly reduces \(Figure 6b\). The inability of the](#)
280 | [assimilation to more strongly reduce the bias is likely due to limited MOPITT observational](#)

Zhe Jiang 6/6/2015 10:30 AM
Deleted: Fig

Zhe Jiang 6/6/2015 10:30 AM
Deleted: (Fig 4a), whereas

Zhe Jiang 6/6/2015 10:30 AM
Deleted: Fig

Zhe Jiang 6/6/2015 10:30 AM
Deleted: Note, that as

Zhe Jiang 6/6/2015 10:30 AM
Deleted: 2014

Zhe Jiang 6/6/2015 10:30 AM
Deleted: Fig

Zhe Jiang 6/6/2015 10:30 AM
Deleted:

Zhe Jiang 6/6/2015 10:30 AM
Deleted: Fig 4d

289 coverage over South America, associated with cloud cover (Keller et al., 2015).

290 A similar bias over the eastern Pacific (0°-12°N, 77.5°W – 122.5°W) was reported by Liu

291 et al. (2010) in their comparison of CO data from the Tropospheric Emission Spectrometer (TES)

292 and GEOS-Chem driven by GEOS-4 and GEOS-5 meteorological fields, for 2005 and 2006 (see

293 their Figures 3 and 4). Relative to TES, the GEOS-Chem was biased high at 681 hPa over the

294 region, which Liu et al. (2010) attributed to excessive export of South American biomass burning

295 emissions, which typically peak in August-September. The magnitude of the bias was larger with

296 GEOS-4 fields than with GEOS-5 (which are used here), and varied from year to year, reflecting

297 the variability in the biomass burning emissions; the model bias was larger in 2005 than in 2006.

298 In Figure 6 we see that relative to MOPITT, the model is biased low in the upper troposphere.

299 This reflects, in part, the high bias in the MOPITT V5J retrievals in the upper troposphere.

300 However, Liu et al. (2010) found that relative to CO data from the Microwave Limb Sounder

301 (MLS), the model (driven by GEOS-5) was also biased low over the eastern Pacific at 215 hPa in

302 August-September 2006, whereas it was biased high in 2005 (see their Figures 5 and 6). The

303 residual bias on the southern boundary will clearly impact the source estimates obtained here,

304 with the high bias in the lower troposphere resulting in an over adjustment (i.e., underestimation)

305 of the CO emission estimates in June – October in southern North America (Mexico and the

306 southern US). Since the TES retrievals are carried out in the presence of clouds, the TES data

307 may provide additional information on CO in the outflow region. Thus, assimilating TES

308 together MOPITT with the Kalman filter may help further reduce the bias the southern boundary

309 conditions. Another promising approach is the weak-constrained 4D-Var technique, recently

310 implemented in GEOS-Chem by Keller et al. (2015), in which the cost function Eq. (2) is

311 augmented with an addition term to mitigate the model transport errors.

312 **4.2. CO Source Estimates for June 2004 – May 2005**

313 Figure 7 shows the monthly scaling factors, which are the ratio of the a posteriori to a
314 priori emissions, for June 2004 – May 2005. The figure shows enhancement of anthropogenic
315 CO emissions in the Great Lakes region and along the US west coast. The annual total
316 anthropogenic emission for the contiguous US 48 states is increased by 14%, from 85 Tg to 97
317 Tg. This estimate is consistent with the results of our global inversion analysis presented in Jiang
318 et al. (2015). The annual total North America CO emission from the oxidation of biogenic VOCs
319 is reduced by 17%, from 61 Tg to 51 Tg with the largest reduction around the Gulf of Mexico in
320 July- September 2004. A possible reason for this reduction is the overestimation of isoprene
321 emission in the MEGANv2.0 inventory used in this work. As discussed in Jiang et al. (2015)
322 several previous studies have suggested that the MEGANv2.0 isoprene emissions are biased high
323 over North America. Hu et al. (2015) found that using the MEGANv2.1, together with an
324 improved land cover distribution, in GEOS-Chem successfully reproduced isoprene observations
325 in North America. However, the MEGANv2.1 inventory is not yet available in the GEOS-Chem
326 adjoint model. It is also possible that the reduction in the biogenic emissions, which are strongest
327 in the southern US, is due, in part, to the high bias in the southern boundary conditions.

328 The time series for the a priori and a posteriori estimates for different emission categories
329 are shown in Figure 8 for all of North America (15°N-65°N) and for the contiguous US 48 states.
330 For the whole continent, generally, the “bottom-up” inventory shows high CO emissions in
331 summer and lower values in winter. This seasonal variation is driven by the oxidation of
332 biogenic VOCs, which is significant in May-September and peaks in July, and by biomass
333 burning, which is at a maximum in April in Mexico and in August in boreal Canada. The
334 uncertainty of the anthropogenic emissions is assumed to be small. The analysis, however, does

Zhe Jiang 6/6/2015 10:30 AM
Deleted: 5

Zhe Jiang 6/6/2015 10:30 AM
Deleted: 2014

Zhe Jiang 6/6/2015 10:30 AM
Deleted: MEGAN 2

Zhe Jiang 6/6/2015 10:30 AM
Deleted: 2014

Zhe Jiang 6/6/2015 10:30 AM
Deleted: MEGAN 2

Zhe Jiang 6/6/2015 10:30 AM
Deleted: Fig 6

341 suggest greater anthropogenic emissions in January-May 2005, which accounts for the larger
342 total CO emissions for this period, as shown in [Figure 8](#).

343 The United States is the largest CO source in North America, contributing 63% to the
344 total North America source. The monthly a priori source in July is 16 Tg, twice as large as the
345 source in winter. The distinct seasonal variation is driven by the strong biogenic VOCs source in
346 summer. During January – April 2005, the total a posteriori CO source in this region is 59 Tg, 36%
347 higher than the a priori value. On the contrary, during June – August 2004, the total a posteriori
348 CO source in this region is 31 Tg, 29% lower than the a priori value. This significant discrepancy
349 between summer and winter was also observed by Kopacz et al. (2010). The estimated winter
350 emissions of Kopacz et al. (2010) are about 50% larger than the summer emissions. Kopacz et al.
351 (2010) and Stein et al. (2014) attributed the [higher wintertime emissions in the Northern](#)
352 [Hemisphere to vehicular emissions, which are not account for in the a priori emission inventory](#).

353 The monthly total CO emissions for the contiguous US 48 states agrees well with the
354 results from the global 4°x5° resolution inversion of Jiang et al. (2015). The largest difference is
355 observed in Dec 2004, when the a posteriori emission estimate from the coarse-resolution
356 inversion is 17% higher. The smallest difference is observed in Oct 2004, when the a posteriori
357 emission estimate of the coarse-resolution inversion is 2% higher. [As discussed in Jiang et al.](#)
358 [\(2015\), the seasonal variations of the a posteriori source estimates obtained here are consistent](#)
359 [with those of Kopcz et al. \(2010\), but the magnitude of the source estimates differ significantly,](#)
360 [reflecting differences in the configuration of the inversions analyses. We refer the reader to](#)
361 [Jiang et al. \(2015\) for a more detailed discussion of the differences between the source estimates](#)
362 [obatined here and those from Kopcz et al. \(2010\).](#)

363 Although there is good agreement at continental scales between our high-resolution

Zhe Jiang 6/6/2015 10:30 AM
Deleted: Fig 6

Zhe Jiang 6/6/2015 10:30 AM
Deleted: low bias of

Zhe Jiang 6/6/2015 10:30 AM
Deleted: CO in winter

Zhe Jiang 6/6/2015 10:30 AM
Deleted: an underestimation of road traffic

Zhe Jiang 6/6/2015 10:30 AM
Deleted: 2014

369 | inverse analysis and the coarse-resolution inversion of Jiang et al. (2015), we do observe
370 | significant differences at regional scales. In June 2004, the high-resolution inversion shows large
371 | changes, along the west coast, whereas the spatial variation is much smaller in the coarse-
372 | resolution inversion, due to averaging on the model grid. More pronounced discrepancies are
373 | observed in Dec 2004. The coarse-resolution inversion shows the a priori CO emission estimates
374 | over Eastern US should be increased by 20-50%. However, the high-resolution inversion shows
375 | much more variation on regional or urban scales. For example, there is a significant CO emission
376 | decrease in the Toronto area, whereas there are large increases to the east of Lake Ontario. There
377 | is also significant CO emission reduction in West Virginia, and large increases in North and
378 | South Carolina. The greater spatial structure in the regional emission estimates is somewhat
379 | expected because of the higher spatial resolution, but it is unclear as to how reliable these
380 | features are, given the information content of the MOPITT data.

381 | The Intercontinental Transport Experiment – North America, Phase A (INTEX-A)
382 | campaign was conducted during July 1 - August 15, 2004, over North America (Singh et al.,
383 | 2006). A DC-8 aircraft was used to measure gas and aerosol abundances, including CO, NO₂,
384 | formaldehyde (HCHO), and H₂O, over an altitude range from 0.2 to 12.5 km. In this work, the
385 | aircraft measurements from the INTEX-A DC-8 aircraft in July 2004 are used to evaluate the
386 | inversion results obtained from MOPITT data. [Figure 9](#) shows the difference between the GEOS-
387 | Chem simulation and the INTEX-A DC-8 aircraft observation in free troposphere. The inverse
388 | model significantly reduces the positive bias in the model bias relative to the aircraft
389 | measurements, from 7.2 ppb to 0.5 ppb, suggesting that the a posteriori CO does indeed provide
390 | a better regional fit to the independent aircraft data. [The reduction in the bias relative to the](#)
391 | [aircraft data also suggests that vertical transport within North America is unbiased, since such a](#)

Zhe Jiang 6/6/2015 10:30 AM

Deleted: 2014

Zhe Jiang 6/6/2015 10:30 AM

Deleted: Fig 7

394 [transport bias in the inversion would degrade the agreement with aircraft data that was obtained](#)
395 [with the optimized initial and boundary conditions \(the a priori\).](#)

396 4.3. Sensitivity of Regional Source Estimates to OH

397 Following Jiang et al. (2015) we assess the sensitivity of the source estimates to the OH
398 fields by repeating the inversion for June – August 2004 with the OH fields from version v8-02-
399 01 of GEOS-Chem. We focus on just the summer months for comparison with Jiang et al. (2015).
400 Also, the OH impact is expected to be greater in summer, when the CO lifetime is short. The
401 initial and boundary conditions for this inversion were obtained by assimilating the MOPITT
402 V5J profiles into the model with the Kalman filter and the v8-02-01 OH fields from 1 January
403 2004 to 1 September 2004. The inversion based on these initial and boundary conditions is
404 referred to as v8OH_BCv8. Our standard inversion with initial and boundary conditions based on
405 the v5-07-08 OH is referred to as v5OH_BCv5. As discussed in Jiang et al. (2015), the OH
406 concentrations in v8-02-01 are significantly higher than the v5-07-08 version in the Northern
407 Hemisphere, and consequently, the CO lifetime is about 30% shorter.

408 Figures [10a-c](#) show the scaling factors for the v8OH_BCv8 inversion. The differences
409 relative to the standard inversion (v5OH_BCv5) are shown in Figs [10d-f](#). The relative difference
410 in the a posteriori CO emission estimates in the contiguous US 48 states inferred from the two
411 OH fields is 32%, suggesting that the OH fields still have a significant impact on the a posteriori
412 estimates, even with the optimized boundary conditions. The relative difference of 32% is 20%
413 smaller than the relative difference (40%) obtained by Jiang et al. (2015) in their 4°x5°
414 resolution global-scale inversion. Although the OH-related error is smaller than in the global,
415 coarse-resolution inversion, it is still suprisingly large. Figures [10j-l](#) show the relative differences
416 between the boundary conditions obtained from the v5-07-08 and the v8-02-01 OH fields, which

Zhe Jiang 6/6/2015 10:30 AM
Deleted: 2014

Zhe Jiang 6/6/2015 10:30 AM
Deleted: 2014

Zhe Jiang 6/6/2015 10:30 AM
Deleted: 2014

Zhe Jiang 6/6/2015 10:30 AM
Deleted: 8a-8c

Zhe Jiang 6/6/2015 10:30 AM
Deleted: 8d-8f

Zhe Jiang 6/6/2015 10:30 AM
Deleted: 2014

Zhe Jiang 6/6/2015 10:30 AM
Deleted: 8j-8l

424 were used in the v5OH_BCv5 and v8OH_BCv8 inversions, respectively. Under ideal conditions,
425 the difference between two boundary conditions should be small because both were optimized
426 with the same MOPITT data using the same approach. However, we do see large differences of
427 more than 15% along the northern and northeastern boundaries, suggesting our optimization of
428 the boundary conditions is inadequate. We believe that the main reason for this is that we
429 neglected MOPITT data at high latitudes (see [Figure 4](#)) to avoid a potential positive bias in the
430 data. Assimilating data from multi-instruments, such as was done by Kopacz et al (2010), could
431 provide better data coverage at high-latitudes, and thus a better constraint on the northern
432 boundary conditions. Moving the northern boundary to lower latitude would be also helpful.

Zhe Jiang 6/6/2015 10:30 AM

Deleted: Fig

433 To quantify the contribution of the differences in the boundary conditions to the
434 differences in the source estimates, we repeated the inversion using the v8-02-01 OH fields, but
435 with the initial and boundary conditions obtained with v5-07-08 OH. This inversion is referred to
436 as v8OH_BCv5. Since the initial and boundary conditions in the v8OH_BCv5 and v5OH_BCv5
437 inversions are identical, the differences in the source estimates obtained from these will reflect
438 only the influence of the OH differences over North America. Figures [10g-i](#) show the differences
439 between v8OH_BCv5 and v5OH_BCv5 (our standard inversion). The relative difference in the a
440 posteriori CO emission estimates for the contiguous US 48 states is only 20%, which is 50%
441 smaller than the relative difference obtained by Jiang et al. ([2015](#)) in their 4°x5° global inversion.
442 The large reduction in the impact of OH on the source estimates compared to the global-scale
443 inversion is encouraging, and demonstrates the potential advantages of high-resolution regional
444 inversion analyses.

Zhe Jiang 6/6/2015 10:30 AM

Deleted: 8g-8i

Zhe Jiang 6/6/2015 10:30 AM

Deleted: 2014

445 **5. Summary**

446 High-resolution CTM simulations have obvious accuracy advantages over coarse

450 resolution simulations, particularly for small-scale processes (e.g., Stroud et al. 2011; [Klich and](#)
451 [Fuelberg](#) 2014; Stock et al. 2014). In this work, we used the adjoint of the nested GEOS-Chem
452 model, at a resolution of $0.5^\circ \times 0.67^\circ$, to constrain North American CO emissions during the
453 period of June 2004 – May 2005. To reduce the potential impact of discrepancies in the modeled
454 OH field on the source estimates, we used the V5J surface level MOPITT retrievals. Our results
455 show that the annual total anthropogenic CO emissions for the contiguous US 48 states should be
456 increased by 14%, from 85 Tg to 97 Tg for 2004 – 2005. The adjustment was mainly caused by
457 an increase in emissions near the Great Lakes and along the west coast. The inversion analysis
458 also suggested that the total CO emissions should be increased by 36% during January – April
459 2005, and decreased by 29% during June – August 2004. This seasonal variation was also
460 observed by Kopacz et al. (2010), and could be associated with an underestimation of road traffic
461 emission in winter (Stein et al. 2014). The inversion results were evaluated with in-situ
462 measurements from the DC-8 aircraft during the INTEX-A campaign in July 2004. The mean
463 bias between the model and the aircraft data in the free troposphere was reduced from 7.2 ppb
464 with the a priori emissions to 0.5 ppb with the a posteriori emissions.

465 Reliable initial and boundary conditions are critical for regional inversion analyses. We
466 used a sequential sub-optimal Kalman filter (Parrington et al. 2008) to assimilate MOPITT CO
467 profiles to optimize the distribution of CO (rather than the emissions) to produce improved initial
468 and lateral boundary conditions for the regional inversion analyses. Because of the restricted
469 domain of the regional analyses, the optimized boundary conditions should significantly reduce
470 the sensitivity of the estimated CO sources to errors in long-range transport and in the OH
471 distribution. [We found that the Kalman filter assimilation significantly improved the initial and](#)
472 [lateral boundary conditions, reducing the bias from -13.3% to 3.5%. However, there was a large](#)

Zhe Jiang 6/6/2015 10:30 AM

Deleted: Kilch et al.

474 residual bias in the southern boundary (near 10°N, between 80°W – 100°W), in the outflow
475 region for biomass burning emissions from South America, which could result in an over
476 adjustment of the CO emissions in Mexico and the southern US. Comparison of the inversion
477 results driven with two different OH fields, from version v5-07-08 and v8-02-01 of GEOS-Chem,
478 produced relative differences in the North American source estimates of 32% for June – August
479 2004. This OH-related difference in the source estimates is about 20% smaller than the
480 differences obtained by Jiang et al. (2015) for the same period in their global-scale inversion
481 analysis.

Zhe Jiang 6/6/2015 10:30 AM
Deleted: 2014

482 Examination of the differences in the boundary conditions based on the two OH fields
483 showed large relative differences (greater than 15%) in the northern and northeastern boundaries,
484 suggesting that our optimization of the boundary conditions was inadequate. In our assimilation
485 of the MOPITT data we neglected data pole-ward of 52° and 40° over land and oceans,
486 respectively, to avoid the influence of a potential high-latitude bias in the data, and we believe
487 that this accounted for the weaker constraint on the northern boundary conditions in the analysis.
488 To assess the influence of the boundary conditions we repeated the inversion with the v8-02-01
489 OH fields using the same initial and boundary conditions from the standard inversion using the
490 v5-07-08 OH. In this case, we estimated a relative difference between the source estimates based
491 on the v8-02-01 and v5-07-08 OH fields of 20%, which is 50% smaller than that reported by
492 Jiang et al. (2015). Thus, our best estimate for North American CO emissions for 2004 – 2005 is
493 97 Tg, with a potential error of 20%, associated with discrepancies in local North America OH.

Zhe Jiang 6/6/2015 10:30 AM
Deleted: 2010

494 Our results demonstrate that high-resolution, regional inversion analyses can reduce the
495 sensitivity of the inferred CO source estimates to errors in long-range transport and in the OH
496 distributions. However, the 20% OH-related discrepancy that we estimated is still large, and

499 could indicate that more stringent constraints on the regional boundary conditions are needed.
500 This may be achieved by integrating data from multiple sources. The OH-related discrepancies
501 could also reflect that fact that in summer, air in the middle and upper troposphere over North
502 America is trapped by a semipermanent anticyclone, which allows greater chemical aging than
503 direct lateral export from the continent (Li et al., 2005; Cooper et al., 2007). Although the
504 MOPITT surface level retrievals have peak sensitivity to CO near the boundary layer, their
505 sensitivity extend up to the middle troposphere (see [Figure 1a](#) of Jiang et al. 2013). Consequently,
506 the inversion analyses could be sensitivite to chemical aging of air in the North American
507 anticyclone. Work is needed to determine the residence time for air in the anticyclone compared
508 to the spatio-temporal variability of the constraints on the North American source estimates
509 provided by the MOPITT surface level retrievals. Improving the source estimates will likely
510 require assimilating sufficient information to obtain a strong constraint on the CO distribution on
511 a timescales shorter than the timescale for chemical aging in the domain. Despite these
512 limitations, we believe that our results show the potential advantages of combining high-
513 resolution regional inversion analyses with global analyses to better quantify regional CO source
514 estimates.

515 **Appendix: Observing System Simulation Experiments (OSSE)**

516 The reliability of the nested inversion is examined with an OSSE for the period June 1-15,
517 2004. In the OSSE, we firstly create pseudo-observations, by archiving model output with CO
518 emission unchanged. In the pseudo-inversion, we reduced the CO emission by 50% and the
519 objective of the OSSE is to observe whether the scaling factors can return to true state (1.0).
520 Figure A1a shows the result of the reference global scale inversion with $4^{\circ}\times 5^{\circ}$ resolution. The a
521 posteriori estimation converges to the true state in all major emission regions. In the nested

Zhe Jiang 6/6/2015 10:30 AM

Deleted: Fig

523 inversion (Figure A1c), the model converges to the true state in Eastern US, whereas the result is
524 noisy in Western US and Canada, which is consistent with the global scale inversion, as shown
525 in Figure A1b. The OSSE demonstrates the nested inversion has similar reliability as the global
526 scale assimilation system.

527 **Acknowledgments.**

528 This work was supported by funding from the Natural Science and Engineering Research
529 Council of Canada, the Canadian Space Agency, and NASA grants NNX10AT42G and
530 NNX11AI54G.

531 **References**

- 532 Arellano, A. F. Jr., Kasibhatla, P. S., Giglio, L., van der Werf, G. R., Randerson, J. T., and
533 Collatz, G. J.: Time dependent inversion estimates of global biomass-burning CO emissions
534 using Measurement of Pollution in the Troposphere (MOPITT) measurements, *J. Geophys.*
535 *Res.*, 111, D09303, doi:10.1029/2005JD006613, 2006.
- 536 Bergamaschi, P., Krol, M., Meirink, J. F., Dentener, F., Segers, A., van Aardenne, J., Monni, S.,
537 Vermeulen, A. T., Schmidt, M., Ramonet, M., C., Yver, Meinhardt, F., Nisbet, E. G., R. E.,
538 Fisher, O'Doherty, S. and Dlugokencky, E. J.: Inverse modeling of European CH₄ emissions
539 2001–2006, *J. Geophys. Res.*, 115, D22309, doi:10.1029/2010JD014180, 2010.
- 540 Brioude, J., Petron, G., Frost, G. J., Ahmadov, R., Angevine, W. M., Hsie, E.-Y., Kim, S.-W.,
541 Lee, S.-H., McKeen, S. A., Trainer, M., Fehsenfeld, F. C., Holloway, J. S., Peischl, J., Ryerson,
542 T. B. and Gurney, K. R.: A new inversion method to calculate emission inventories without a
543 prior at mesoscale: Application to the anthropogenic CO₂ emission from Houston, Texas, *J.*
544 *Geophys. Res.*, 117, D05312, doi:10.1029/2011JD016918, 2012.
- 545 Chen, D., Wang, Y., McElroy, M. B., He, K., Yantosca, R. M., and Le Sager, P.: Regional CO

546 pollution and export in China simulated by the high-resolution nested-grid GEOS-Chem model,
547 Atmos. Chem. Phys., 9, 3825-3839, doi:10.5194/acp-9-3825-2009, 2009.

548 Cooper, O. R., et al., Evidence for a recurring eastern North America upper tropospheric ozone
549 maximum during summer, J. Geophys. Res., 112, D23304, doi:10.1029/2007JD008710, 2007.

550 Corazza, M., Bergamaschi, P., Vermeulen, A. T., Aalto, T., Haszpra, L., Meinhardt, F.,
551 O'Doherty, S., Thompson, R., Moncrieff, J., Popa, E., Steinbacher, M., Jordan, A.,
552 Dlugokencky, E., Brühl, C., Krol, M., and Dentener, F.: Inverse modelling of European N₂O
553 emissions: assimilating observations from different networks, Atmos. Chem. Phys., 11, 2381-
554 2398, doi:10.5194/acp-11-2381-2011, 2011..

555 Curci, G., Palmer, P. I., Kurosu, T. P., Chance, K., and Visconti, G.: Estimating European
556 volatile organic compound emissions using satellite observations of formaldehyde from the
557 Ozone Monitoring Instrument, Atmos. Chem. Phys., 10, 11501-11517, doi:10.5194/acp-10-
558 11501-2010, 2010.

559 Deeter, M. N., Worden, H. M., Gille, J. C., Edwards, D. P., Mao, D., and Drummond, J. R.:
560 MOPITT multispectral CO retrievals: Origins and effects of geophysical radiance errors, J.
561 Geophys. Res., 116, D15303, doi:10.1029/2011JD015703, 2011.

562 Deeter, M. N., Worden, H. M., Edwards, D. P., Gille, J. C., and Andrews, A. E.: Evaluation of
563 MOPITT retrievals of lower-tropospheric carbon monoxide over the United States, J. Geophys.
564 Res., 117, D13306, doi:10.1029/2012JD017553, 2012.

565 Deeter, M. N., Martínez-Alonso, S., Edwards, D. P., Emmons, L. K., Gille, J. C., Worden, H. M.,
566 Pittman, J. V., Daube, B. C., and Wofsy, S. C.: Validation of MOPITT Version 5 thermal-
567 infrared, near-infrared, and multispectral carbon monoxide profile retrievals for 2000–2011, J.
568 Geophys. Res. Atmos., 118, 6710–6725, doi:10.1002/jgrd.50272, 2013.

569 Deng, F., et al., Inferring regional sources and sinks of atmospheric CO₂ from GOSAT XCO₂
570 data, *Atmos. Chem. Phys.*, 14, 3703-3727, doi:10.5194/acp-14-3703-2014, 2014.

571 Evans, M. J., and Jacob, D. J.: Impact of new laboratory studies of N₂O₅ hydrolysis on global
572 model budgets of tropospheric nitrogen oxides, ozone, and OH, *Geophys. Res. Lett.*, 32,
573 L09813, doi:10.1029/2005GL022469, 2005.

574 Fortems-Cheiney, A., Chevallier, F., Pison, I., Bousquet, P., Szopa, S., Deeter, M. N., and
575 Clerbaux, C.: Ten years of CO emissions as seen from Measurements of Pollution in the
576 Troposphere (MOPITT), *J. Geophys. Res.*, 116, D05304, doi:10.1029/2010JD014416, 2011.

577 Fortems-Cheiney, A., Chevallier, F., Pison, I., Bousquet, P., Saunois, M., Szopa, S., Cressot, C.,
578 Kurosu, T. P., Chance, K., and Fried, A.: The formaldehyde budget as seen by a global-scale
579 multi-constraint and multi-species inversion system, *Atmos. Chem. Phys.*, 12, 6699-6721,
580 doi:10.5194/acp-12-6699-2012, 2012.

581 Göckede, M., Turner, D. P., Michalak, A. M., Vickers, D., and Law, B. E.: Sensitivity of a
582 subregional scale atmospheric inverse CO₂ modeling framework to boundary conditions, *J.*
583 *Geophys. Res.*, 115, D24112, doi:10.1029/2010JD014443, 2010.

584 Gonzi, S., Feng, L., and Palmer, P. I.: Seasonal cycle of emissions of CO inferred from MOPITT
585 profiles of CO: Sensitivity to pyroconvection and profile retrieval assumptions, *Geophys. Res.*
586 *Lett.*, 38, L08813, doi:10.1029/2011GL046789, 2011.

587 Heald, C. L., Jacob, D. J., Jones, D. B. A., Palmer, P. I., Logan, J. A., Streets, D. G., Sachse, G.
588 W., Gille, J. C., Hoffman, R. N., and Nehr Korn, T.: Comparative inverse analysis of satellite
589 (MOPITT) and aircraft (TRACE-P) observations to estimate Asian sources of carbon monoxide,
590 *J. Geophys. Res.* 109, D23306, doi:10.1029/2004JD005185, 2004.

591 Henze, D. K., Hakami, A., and Seinfeld, J. H.: Development of the adjoint of GEOS- Chem,

592 Atmos. Chem. Phys., 7, 2413–2433, doi:10.5194/acp-7-2413-2007, 2007.

593 Jiang, Z., D. Jones, B. A., Kopacz, M., Liu, J., Henze, D. K., and Heald, C., Quantifying the
594 impact of model errors on top-down estimates of carbon monoxide emissions using satellite
595 observations, J. Geophys. Res., 116, D15306, doi:10.1029/2010JD015282, 2011.

596 Jiang, Z., Jones, D. B. A., Worden, H. M., Deeter, M. N., Henze, D. K., Worden, J., Bowman, K.
597 W., Brenninkmeijer, C. A. M., and Schuck, T. J.: Impact of model errors in convective
598 transport on CO source estimates inferred from MOPITT CO retrievals, J. Geophys. Res.
599 Atmos., 118, 2073–2083, 2013.

600 Jiang, Z., Jones, D. B. A., Worden, H. M., and Henze, D. K.: Sensitivity of top-down CO source
601 estimates to the modeled vertical structure in atmospheric CO, Atmos. Chem. Phys., 15, 1521-
602 1537, doi:10.5194/acp-15-1521-2015, 2015.

603 Jones, D. B. A., Bowman, K. W., Logan, J. A., Heald, C. L., Liu, J., Luo, M., Worden, J., and
604 Drummond, J.: The zonal structure of tropical O₃ and CO as observed by the Tropospheric
605 Emission Spectrometer in November 2004 – Part 1: Inverse modeling of CO emissions, Atmos.
606 Chem. Phys., 9, 3547 – 3562, 2009.

607 Keller, M., Jones, D. B. A., Jiang, Z., Henze, D. K., Worden, H. M.: Quantifying Model Biases
608 in CO Emission Estimation Using Weak Constraint 4D-Var, submitted to J. Geophys. Res.,
609 2015.

610 Klich, C. A. and Fuelberg, H. E.: The role of horizontal model resolution in assessing the
611 transport of CO in a middle latitude cyclone using WRF-Chem, Atmos. Chem. Phys., 14, 609-
612 627, doi:10.5194/acp-14-609-2014, 2014.

613 Kopacz, M., Jacob, D., Henze, D., Heald, C., Streets, D. and Zhang, Q.: Comparison of adjoint
614 and analytical Bayesian inversion methods for constraining Asian sources of carbon monoxide

Zhe Jiang 6/6/2015 10:30 AM

Deleted: inferred regional

Zhe Jiang 6/6/2015 10:30 AM

Formatted: Indent: Left: 0", Hanging: 0.59 ch, First line: -0.59 ch

Zhe Jiang 6/6/2015 10:30 AM

Deleted: as observed by MOPITT

Zhe Jiang 6/6/2015 10:30 AM

Deleted: . Discuss., 14, 22939-22984

Zhe Jiang 6/6/2015 10:30 AM

Deleted: acpd-14-22939-2014, 2014

619 | [using satellite \(MOPITT\) measurements of CO columns, J. Geophys. Res., 114\(D4\),](#)
620 | [doi:10.1029/2007JD009264, 2009.](#)
621 | [Kopacz, M., Jacob, D. J., Fisher, J. A., Logan, J. A., Zhang, L., Megretskaia, I. A., Yantosca, R.](#)
622 | [M., Singh, K., Henze, D. K., Burrows, J. P., Buchwitz, M., Khlystova, I., McMillan, W. W.,](#)
623 | [Gille, J. C., Edwards, D. P., Eldering, A., Thouret, V. and Nedelec, P.:](#) Global estimates of CO
624 | sources with high resolution by adjoint inversion of multiple satellite datasets (MOPITT, AIRS,
625 | SCIAMACHY, TES), *Atmos. Chem. Phys.*, 10, 855-876, doi:10.5194/acp-10-855-2010, 2010.
626 | Lauvaux, T., Schuh, A. E., Uliasz, M., Richardson, S., Miles, N., Andrews, A. E., Sweeney, C.,
627 | Diaz, L. I., Martins, D., Shepson, P. B., and Davis, K. J.: Constraining the CO₂ budget of the
628 | corn belt: exploring uncertainties from the assumptions in a mesoscale inverse system, *Atmos.*
629 | *Chem. Phys.*, 12, 337-354, doi:10.5194/acp-12-337-2012, 2012.
630 | Liu, D. C. and J. Nocedal, On the Limited Memory Method for Large Scale Optimization,
631 | *Mathematical Programming*, 45, 503-528, [1989](#).
632 | Liu, J.-H., Logan, J. A., Jones, D. B. A., Livesey, N. J., Megretskaia, I., Carouge, C. and Nedelec,
633 | P.: Analysis of CO in the tropical troposphere using Aura satellite data and the GEOS-Chem
634 | model: insights into transport characteristics of the GEOS meteorological products, *Atmos.*
635 | *Chem. Phys.*, 10, 12207-12232, doi:10.5194/acp-10-12207-2010, 2010.
636 | Locatelli, R., Bousquet, P., Chevallier, F., Fortems-Cheney, A., Szopa, S., Saunois, M., Agusti-
637 | Panareda, A., Bergmann, D., Bian, H., Cameron-Smith, P., Chipperfield, M. P., Gloor, E.,
638 | Houweling, S., Kawa, S. R., Krol, M., Patra, P. K., Prinn, R. G., Rigby, M., Saito, R., and
639 | Wilson, C.: Impact of transport model errors on the global and regional methane emissions
640 | estimated by inverse modelling, *Atmos. Chem. Phys.*, 13, 9917-9937, doi:10.5194/acp-13-
641 | 9917-2013, 2013.

Zhe Jiang 6/6/2015 10:30 AM

Deleted: 2010

643 Meirink, J. F., Bergamaschi, P., and Krol, M. C.: Four-dimensional variational data assimilation
644 for inverse modelling of atmospheric methane emissions: method and comparison with
645 synthesis inversion, *Atmos. Chem. Phys.*, 8, 6341-6353, doi:10.5194/acp-8-6341-2008, 2008.

646 [Palmer, P., Jacob, D., Jones, D., Heald, C., Yantosca, R., Logan, J., Sachse, G. and Streets, D.:](#)
647 [Inverting for emissions of carbon monoxide from Asia using aircraft observations over the](#)
648 [western Pacific, *J. Geophys. Res.*, 108\(D21\), doi:10.1029/2003JD003397, 2003.](#)

649 Parrington, M., Jones, D. B. A., Bowman, K. W., Horowitz, L. W., Thompson, A. M., Tarasick,
650 D. W., and Witte, J. C.: Estimating the summertime tropospheric ozone distribution over North
651 America through assimilation of observations from the Tropospheric Emission Spectrometer, *J.*
652 *Geophys. Res.*, 113, D18307, doi:10.1029/2007JD009341, 2008.

653 Parrington, M., Palmer, P. I., Henze, D. K., Tarasick, D. W., Hyer, E. J., Owen, R. C., Helmig,
654 D., Clerbaux, C., Bowman, K. W., Deeter, M. N., Barratt, E. M., Coheur, P.-F., Hurtmans, D.,
655 Jiang, Z., George, M. and Worden, J. R.: The influence of boreal biomass burning emissions on
656 the distribution of tropospheric ozone over North America and the North Atlantic during
657 2010, *Atmos. Chem. Phys.*, 12, 2077-2098, doi:10.5194/acp-12-2077-2012, 2012.

658 Pétron, G., Granier, C., Khattatov, B., Yudin, V., Lamarque, J.-F., Emmons, L., Gille, J., and
659 Edwards, D. P.: Monthly CO surface sources inventory based on the 2000– 2001 MOPITT
660 satellite data, *Geophys. Res. Lett.*, 31, L21107, doi:10.1029/2004GL020560, 2004.

661 Peylin, P., Houweling, S., Krol, M. C., Karstens, U., Rödenbeck, C., Geels, C., Vermeulen, A.,
662 Badawy, B., Aulagnier, C., Pregger, T., Delage, F., Pieterse, G., Ciais, P., and Heimann, M.:
663 Importance of fossil fuel emission uncertainties over Europe for CO₂ modeling: model
664 intercomparison, *Atmos. Chem. Phys.*, 11, 6607-6622, doi:10.5194/acp-11-6607-2011, 2011.

665 Singh, H. B., Brune, W. H., Crawford, J. H., Jacob, D. J., and Russell, P. B.: Overview of the

666 summer 2004 Intercontinental Chemical Transport Experiment– North America (INTEX-A), *J.*
667 *Geophys. Res.*, 111, D24S01, doi:10.1029/2006JD007905, 2006.

668 Singh, K., Jardak, M., Sandu, A., Bowman, K., Lee, M., and Jones, D.: Construction of non-
669 diagonal background error covariance matrices for global chemical data assimilation, *Geosci.*
670 *Model Dev.*, 4, 299-316, doi:10.5194/gmd-4-299-2011, 2011.

671 Stein, O., Schultz, M. G., Bouarar, I., Clark, H., Huijnen, V., Gaudel, A., George, M., and
672 Clerbaux, C.: On the wintertime low bias of Northern Hemisphere carbon monoxide found in
673 global model simulations, *Atmos. Chem. Phys.*, 14, 9295-9316, doi:10.5194/acp-14-9295-2014,
674 2014.

675 Stock, Z. S., Russo, M. R., and Pyle, J. A.: Representing ozone extremes in European megacities:
676 the importance of resolution in a global chemistry climate model, *Atmos. Chem. Phys.*, 14,
677 3899-3912, doi:10.5194/acp-14-3899-2014, 2014.

678 Stroud, C. A., Makar, P. A., Moran, M. D., Gong, W., Gong, S., Zhang, J., Hayden, K., Mihele,
679 C., Brook, J. R., Abbatt, J. P. D., and Slowik, J. G.: Impact of model grid spacing on regional-
680 and urban- scale air quality predictions of organic aerosol, *Atmos. Chem. Phys.*, 11, 3107-3118,
681 doi:10.5194/acp-11-3107-2011, 2011.

682 Valin, L. C., Russell, A. R., Hudman, R. C., and Cohen, R. C.: Effects of model resolution on the
683 interpretation of satellite NO₂ observations, *Atmos. Chem. Phys.*, 11, 11647-11655,
684 doi:10.5194/acp-11-11647-2011, 2011.

685 Wang, Y. X., McElroy, M. B., Jacob, D. J., and Yantosca, R. M.: A nested grid formulation for
686 chemical transport over Asia: Applications to CO, *J. Geophys. Res.*, 109, D22307,
687 doi:10.1029/2004JD005237, 2004.

688 Wecht, K. J., Jacob, D. J., Sulprizio, M. P., Santoni, G. W., Wofsy, S. C., Parker, R., Bösch, H.,

689 and Worden, J.: Spatially resolving methane emissions in California: constraints from the
690 CalNex aircraft campaign and from present (GOSAT, TES) and future (TROPOMI,
691 geostationary) satellite observations, *Atmos. Chem. Phys.*, 14, 8173-8184, doi:10.5194/acp-14-
692 8173-2014, 2014.

693 Wells, K.C., et al., Quantifying global terrestrial methanol emissions using observations from the
694 TES satellite sensor, *Atmos. Chem. Phys.*, 14, 2555-2570, doi:10.5194/acp-14-2555-2014,
695 2014.

696 Worden, H. M., Deeter, M. N., Edwards, D. P., Gille, J. C., Drummond, J. R., and Nédélec, P.:
697 Observations of near-surface carbon monoxide from space using MOPITT multispectral
698 retrievals, *J. Geophys. Res.*, 115, D18314, doi:10.1029/2010JD014242, 2010.

699 Worden, J., et al., El Niño, the 2006 Indonesian peat fires, and the distribution of atmospheric
700 methane, *Geophys. Res. Lett.*, 40, 4938-4943, doi:10.1002/grl.50937, 2013.

701

702 **Tables and Figures**

703 **Figure 1.** Annual mean CO emissions from fossil fuel (FF), biofuel (BF), biomass burning (BB)
704 and the oxidation of biogenic NMVOC and CH₄, averaged for June 2004 to May 2005. The unit
705 is 10¹² molec/cm²/sec.

706

707 **Figure 2.** CO mixing ratio in GEOS-Chem on level 10 (about 850 hPa) on May 1, 2006. The
708 influence of a mid-latitude cyclone is clearly shown in the high-resolution (0.5°x0.667°)
709 simulation (right), whereas it is not obvious in that with coarse resolution (4°x5°) simulation
710 (left). The light yellow line on the 0.5°x0.667° plot demarcates the buffer zone in which the
711 coarse resolution boundary conditions are imposed.

712

713 **Figure 3.** Relative difference between the optimized lower tropospheric partial columns (surface
714 – 500 hPa) between Kalman Filter assimilation, referred as CO_KF and a posteriori simulation
715 of global scale inversion, referred as CO_EMS. The value is calculated as (CO_EMS – CO_KF)
716 / CO_KF.

717

718 **Figure 4.** Mean tropospheric CO columns (10¹⁸ molec/cm²) in the GEOS-Chem North America
719 nested domain in June 2004 from (a) MOPITT version 5; (b) GEOS-Chem model with the
720 original initial and boundary conditions; (c) with the optimized initial and boundary conditions.

721 | Note that MOPITT data poleward of 40° and 52° over oceans and land, respectively, are not used
722 | in this work to reduce the influence of potential positive bias in MOPITT CO retrievals, as
723 | described in Jiang et al. (2015).

725 | **Figure 5.** Distribution of the relative bias between the model and MOPITT with the original
726 | initial and lateral boundary conditions (red) and the optimized initial and lateral boundary
727 | conditions (blue), after assimilation of the MOPITT data using the Kalman filter. The numbers
728 | are the mean relative difference.

730 | **Figure 6.** Vertical distribution of relative difference in June 2004 along the southern boundary,
731 | between model and MOPITT, calculated as (Mod - MOP) / MOP. (a) original model simulation,
732 | (b) optimized model simulation by assimilating MOPITT data using Kalman Filter.

734 | **Figure 7.** Monthly scaling factor for total CO emissions (from combustion sources and the
735 | oxidation of biogenic NMVOC) during June 2004 – May 2005.

737 | **Figure 8.** Monthly CO emissions during June 2004 – May 2005 for different emission
738 | categories: total emissions (black), anthropogenic emissions (blue), biomass burning (red), and
739 | the oxidation of biogenic NMVOCs (green). The a priori estimates are shown with the solid line
740 | and a posteriori values are indicated with the dashed line. The unit is Tg/month.

742 | **Figure 9.** Difference between the GEOS-Chem simulation with INTEX-A DC-8 aircraft
743 | observation in free troposphere in July 2004. (a) A priori model simulation, (based on the
744 | optimized initial and boundary conditions). (b) A posteriori model simulation. The model is
745 | sampled at the aircraft measurements time, location and altitude.

747 | **Figure 10.** (a–c): Scaling factors of v8OH_BCv8 inversion, based on the v8-02-01 OH; (d–f):
748 | Difference between scaling factors of the v5OH_BCv5 and v8OH_BCv8 inversions; (g–i):
749 | Similar to Panel (d–f), but for the v8OH_BCv5 inversion, with the initial and boundary
750 | conditions from the standard inversion with the v5-07-08 OH fields; (j–l) Relative difference
751 | between the lower tropospheric CO partial columns (surface – 500 hPa) of the boundary
752 | conditions for the v5OH_BCv5 (v5) and the v8OH_BCv8 (v8) inversions, calculated as: $2 * (v8$
753 | $- v5) / (v8 + v5)$.

755 | **Figure A1.** OSSE scaling factors for June 1-15, 2004. (a) Global reference inversion with 4°x5°
756 | resolution. (b) Zoomed in North America region of the global inversion. (c) Nested inversion
757 | results. The scaling factor for the first guess is 0.5 and for the true state is 1.0.

Zhe Jiang 6/6/2015 10:30 AM
Deleted: (d) Relative difference, (Mod - MOP) / MOP, using original (Red), and optimized (Blue) initial and boundary conditions. The numbers in Panel (d) are mean bias.
Zhe Jiang 6/6/2015 10:30 AM
Deleted: 2014
Zhe Jiang 6/6/2015 10:30 AM
Formatted: English (US)
Zhe Jiang 6/6/2015 10:30 AM
Deleted: Figure 5.

Zhe Jiang 6/6/2015 10:30 AM
Deleted: 6

Zhe Jiang 6/6/2015 10:30 AM
Deleted: 7
Zhe Jiang 6/6/2015 10:30 AM
Deleted: .

Zhe Jiang 6/6/2015 10:30 AM
Formatted: English (CAN)
Zhe Jiang 6/6/2015 10:30 AM
Formatted: Indent: Left: 0", First line: 0 ch, Line spacing: single, Widow/Orphan
Zhe Jiang 6/6/2015 10:30 AM
Deleted: 8

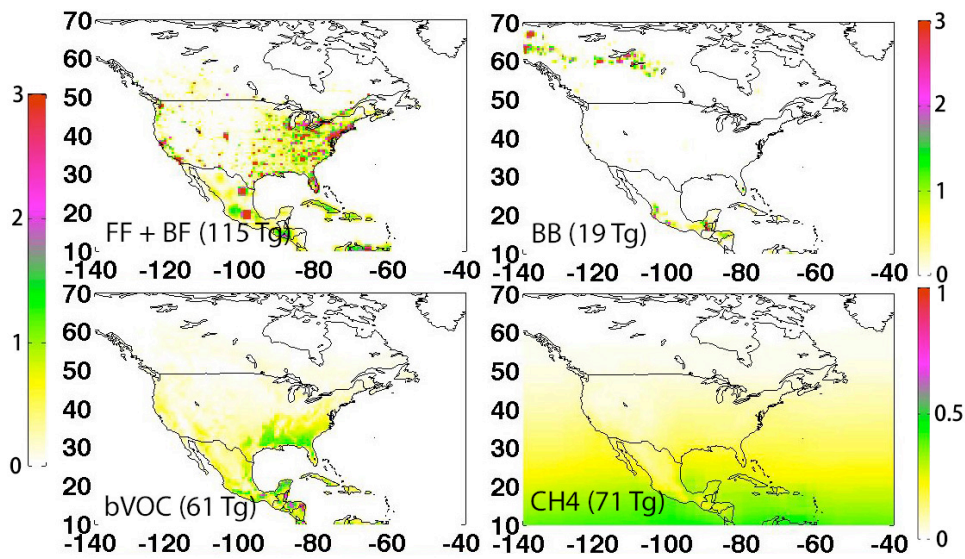


Figure 1. Annual mean CO emissions from fossil fuel (FF), biofuel (BF), biomass burning (BB) and the oxidation of biogenic NMVOC and CH₄, averaged for June 2004 to May 2005. The unit is 10¹² molec/cm²/sec.

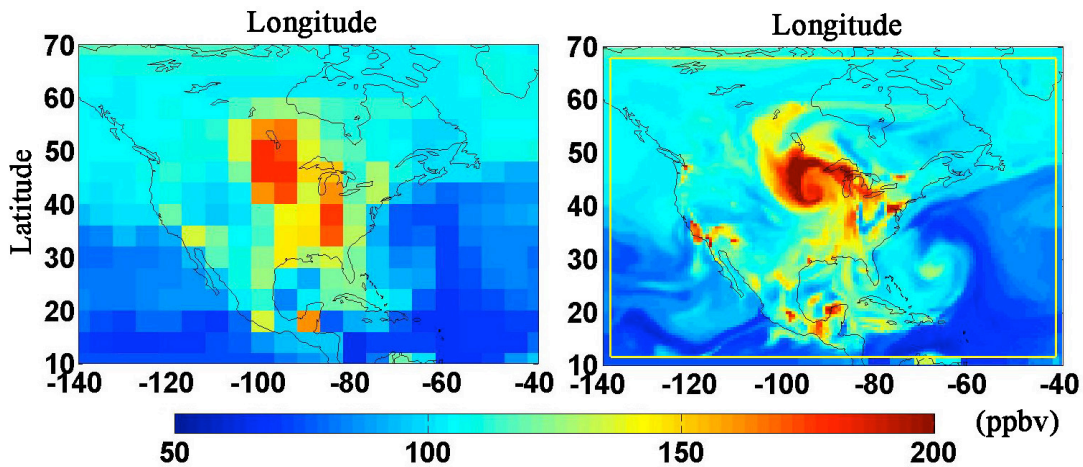


Figure 2. CO mixing ratio in GEOS-Chem on level 10 (about 850 hPa) on May 1, 2006. The influence of a mid-latitude cyclone is clearly shown in the high-resolution (0.5°x0.667°) simulation (right), whereas it is not obvious in that with coarse resolution (4°x5°) simulation (left). The light yellow line on the 0.5°x0.667° plot demarcates the buffer zone in which the coarse resolution boundary conditions are imposed.

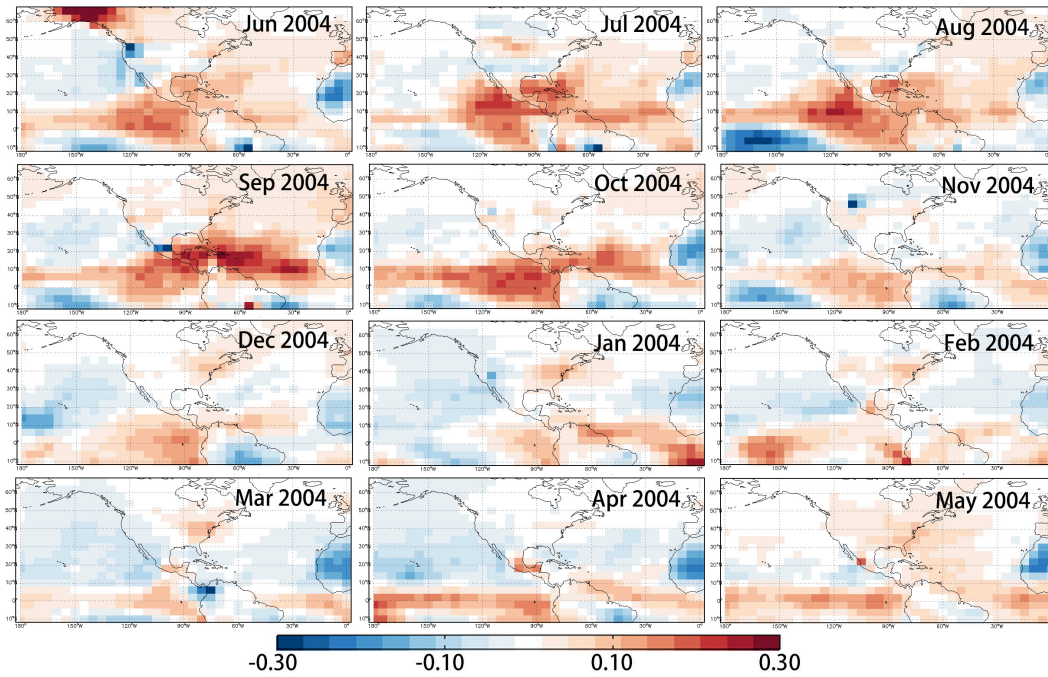


Figure 3. Relative difference between the optimized lower tropospheric partial columns (surface – 500 hPa) between Kalman Filter assimilation, referred as CO_KF and a posteriori simulation of global scale inversion, referred as CO_EMS. The value is calculated as $(CO_EMS - CO_KF) / CO_KF$.

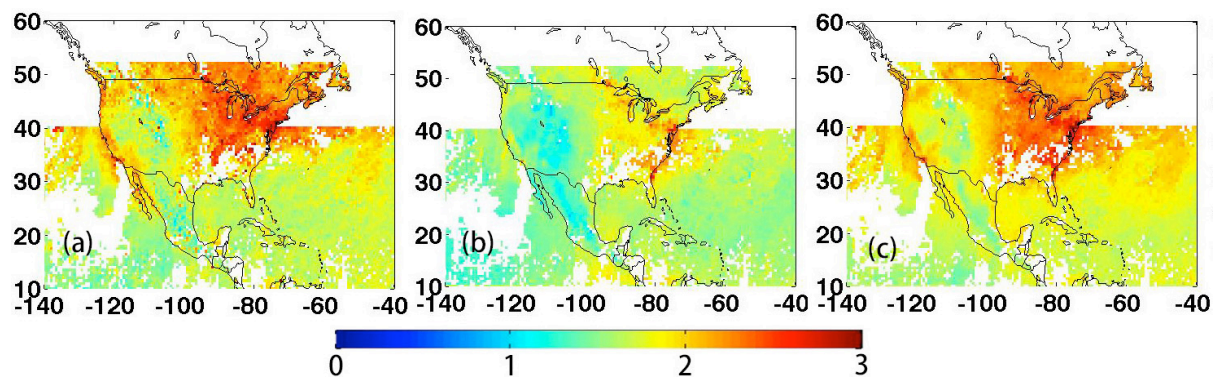


Figure 4. Mean tropospheric CO columns (10^{18} molec/cm²) in the GEOS-Chem North America nested domain in June 2004 from (a) MOPITT version 5; (b) GEOS-Chem model with the original initial and boundary conditions; (c) with the optimized initial and boundary conditions. Note that MOPITT data poleward of 40° and 52° over oceans and land, respectively, are not used in this work to reduce the influence of potential positive bias in MOPITT CO retrievals, as described in Jiang et al. (2015).

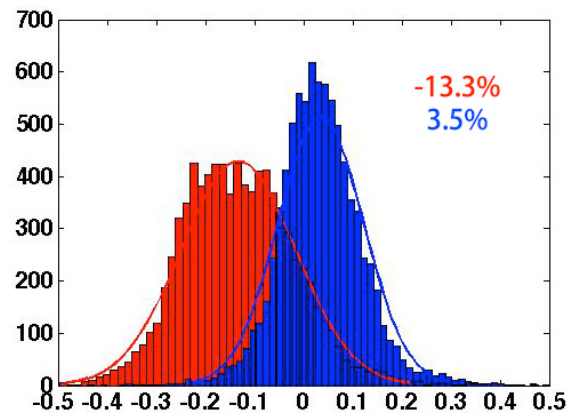


Figure 5. Distribution of the relative bias between the model and MOPITT with the original initial and lateral boundary conditions (red) and the optimized initial and lateral boundary conditions (blue), after assimilation of the MOPITT data using the Kalman filter. The numbers are the mean relative difference.

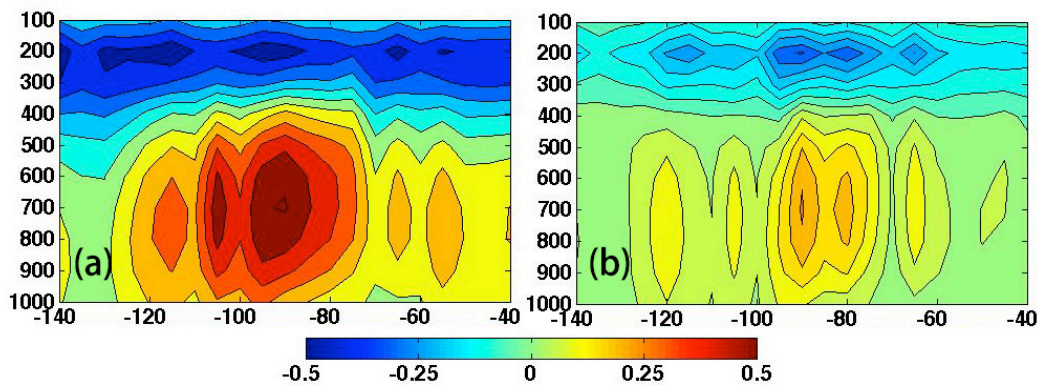


Figure 6. Vertical distribution of relative difference in June 2004 along the southern boundary, between model and MOPITT, calculated as $(\text{Mod} - \text{MOP}) / \text{MOP}$. (a) original model simulation. (b) optimized model simulation by assimilating MOPITT data using Kalman Filter.

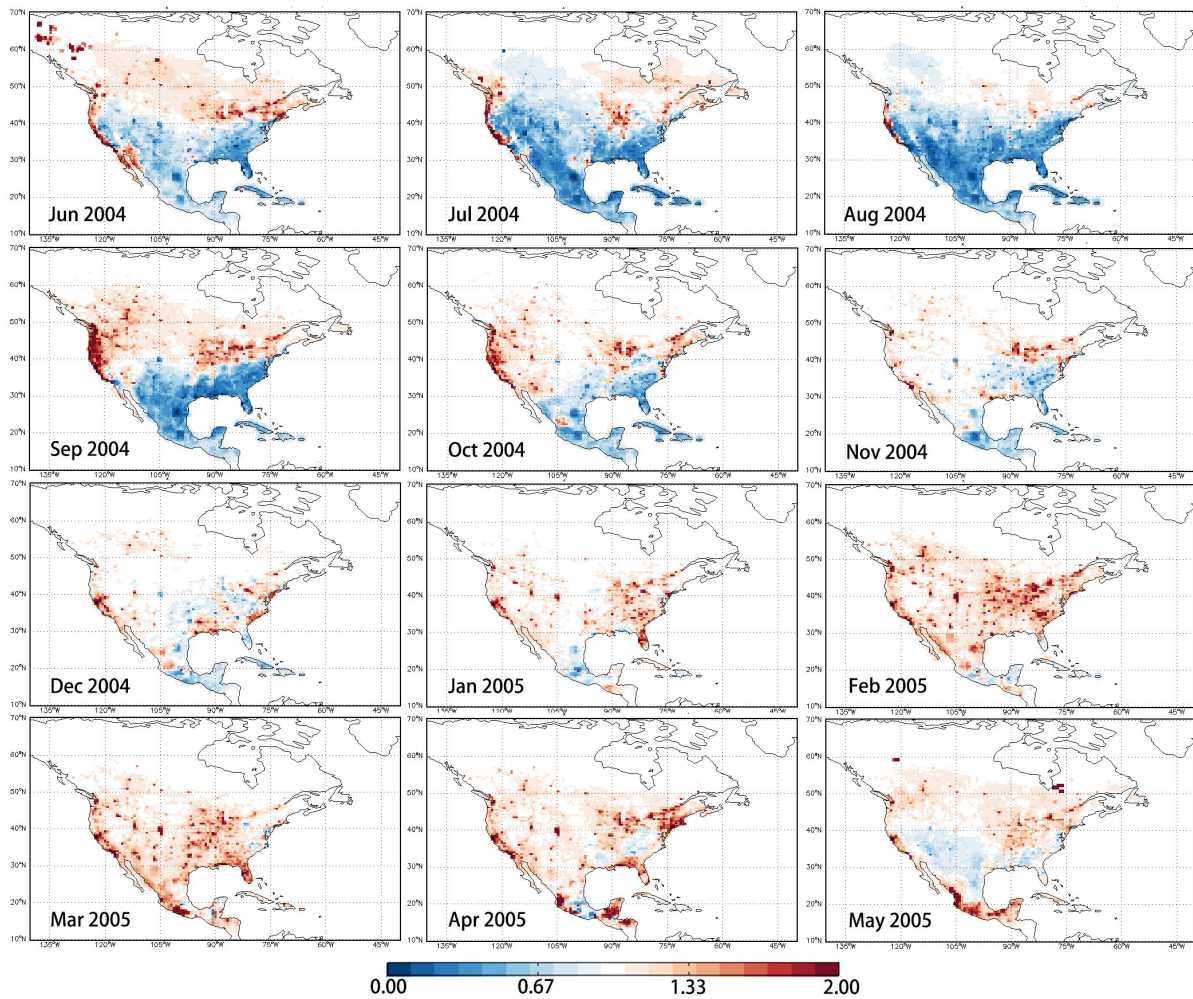


Figure 7. Monthly scaling factor for total CO emissions (from combustion sources and the oxidation of biogenic NMVOC) during June 2004 – May 2005.

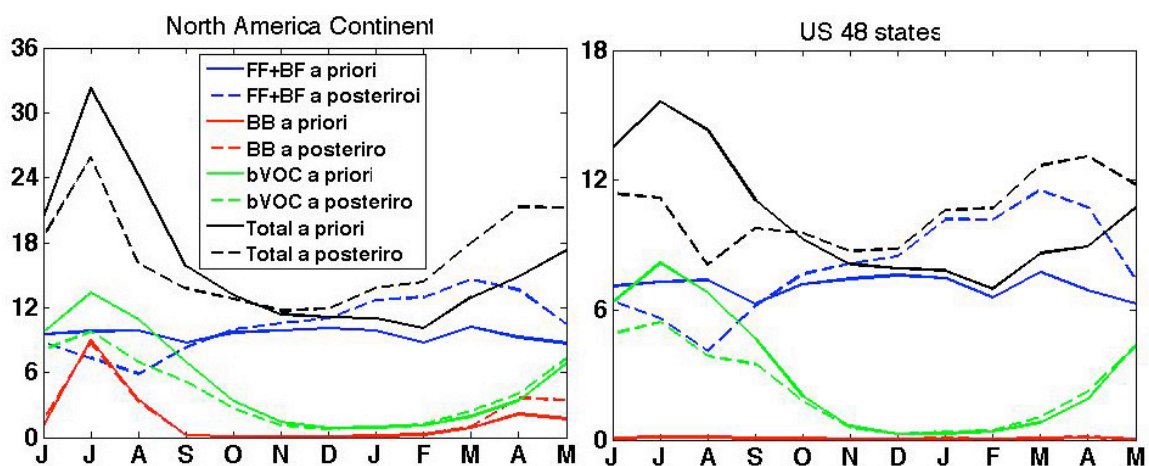


Figure 8. Monthly CO emissions during June 2004 – May 2005 for different emission categories: total emissions (black), anthropogenic emissions (blue), biomass burning (red), and the oxidation of biogenic NMVOCs (green). The a priori estimates are shown with the solid line and a posteriori values are indicated with the dashed line. The unit is Tg/month.

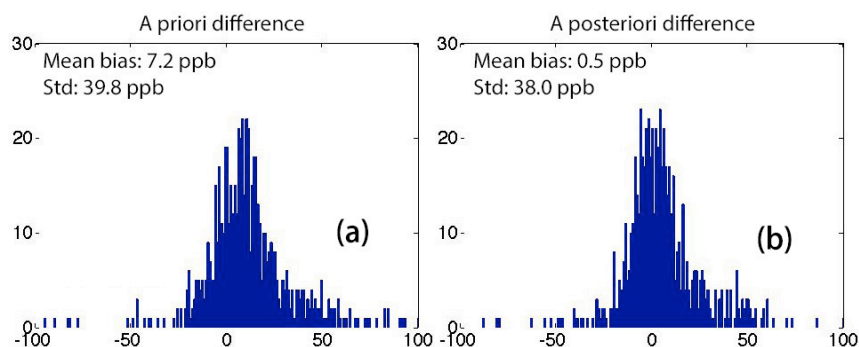


Figure 9. Difference between the GEOS-Chem simulation with INTEX-A DC-8 aircraft observation in free troposphere in July 2004. (a) A priori model simulation (based on the optimized initial and boundary conditions). (b) A posteriori model simulation. The model is sampled at the aircraft measurements time, location and altitude.

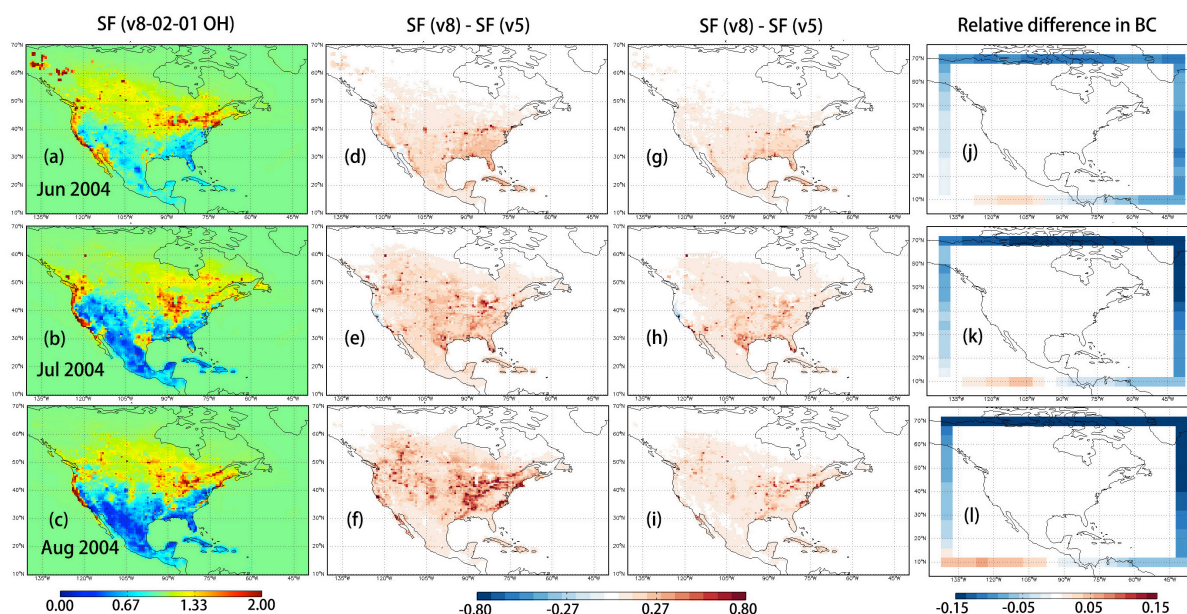


Figure 10. (a–c): Scaling factors of v8OH_BCv8 inversion, based on the v8-02-01 OH; (d–f): Difference between scaling factors of the v5OH_BCv5 and v8OH_BCv8 inversions; (g–i): Similar to Panel (d–f), but for the v8OH_BCv5 inversion, with the initial and boundary conditions from the standard inversion with the v5-07-08 OH fields; (j–l) Relative difference between the lower tropospheric CO partial columns (surface – 500 hPa) of the boundary conditions for the v5OH_BCv5 (v5) and the v8OH_BCv8 (v8) inversions, calculated as: $2 * (v8 - v5) / (v8 + v5)$.

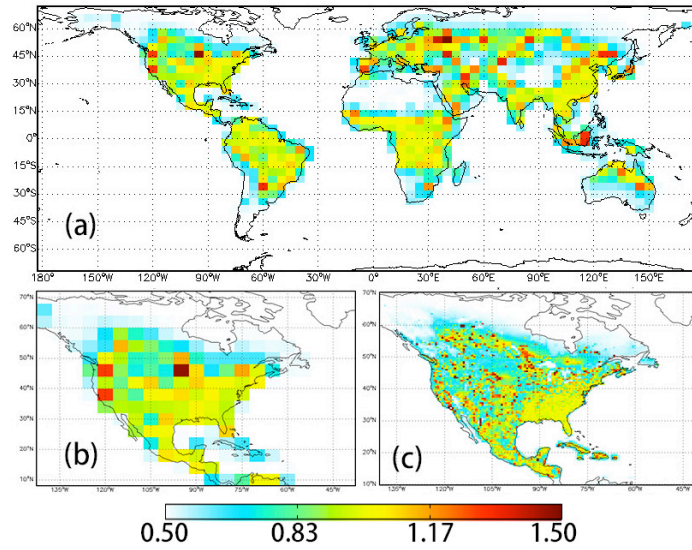


Figure A1. OSSE scaling factors for June 1-15, 2004. (a) Global reference inversion with $4^\circ \times 5^\circ$ resolution. (b) Zoomed in North America region of the global inversion. (c) Nested inversion results. The scaling factor for the first guess is 0.5 and for the true state is 1.0.